A Vacuum Ultraviolet Photoionization Mass Spectrometric Study of Propylene Oxide in the Photon Energy Region of 10−40 eV

Fuyi Liu, Luisi Sheng, Fei Qi, Hui Gao, Chengxiang Li, and Yunwu Zhang

National Synchrotron Radiation Laboratory, University of Science and Technology of China, Hefei, Anhui, 230026 People's Republic of China

Shuqin Yu

Department of Chemical Physics, University of Science and Technology of China, Hefei, Anhui, 230026 People's Republic of China

Kai-Chung Lau and Wai-Kee Li*

Department of Chemistry, The Chinese University of Hong Kong, Shatin, N.T., Hong Kong

Received: February 23, 1999; In Final Form: May 27, 1999

The photoionization and dissociative photoionizations of propylene oxide have been studied both experimentally and theoretically. In experiments, photoionization efficiency spectra for ions $C_3H_6O^+$, $C_2H_3O^+$, CH_3O^+, CH_2O^+, CHO^+, $C_2H_4^+$, $C_2H_3^+$, $C_2H_2^+$, CH_3^+, and CH_2^+ were obtained. Theoretically, the energetics of the dissociative photoionizations were examined by ab initio Gaussian-2 calculations. The computational results are useful in our attempt to establish the dissociation channels near the ionization thresholds. The dissociation channels we propose include simple bond cleavage reactions as well as reactions involving intermediates and transition structures.

Introduction

Epoxides are important and interesting compounds. Structurally, there are polar covalent bonds in the three-membered ring and there is strong ring strain as well. Thus, these compounds undergo ring-opening reactions easily. Also, it has been established that the epoxy functional group plays an important role in the biological activities of a large number of natural products.[1] Hence, quantitative studies on the various dissociations of epoxy compounds are clearly desirable. In an earlier work,[2] by means of both experiments and high-level computations, we proposed the dissociation channels of ethylene oxide near the ionization thresholds. In the present work, we employ similar techniques to determine the energetics of the photoionization and dissociative photoionizations of propylene oxide. It is noted that propylene oxide is structurally less symmetric than ethylene oxide and hence these two compounds have different dissociation products.

Previously, Gallegos and Kiser[3] measured the ionization and dissociative ionizations of propylene oxide with time-of-flight mass spectrometry (TOF-MS) by the electron impact (EI) technique. They reported the appearance energies (AEs) of the principal cations in the mass spectra of propylene oxide and gave probable dissociation processes. To our knowledge, the dissociative photoionizations of propylene oxide with TOF-MS have not been reported in the literature. On the other hand, the ionization energy (IE) of propylene oxide was measured by various groups using photoelectron[4−6] and photoionization[7] spectroscopy, in addition to the EI measurement previously mentioned.[3] However, the IEs these groups reported are rather scattered, ranging from 9.8 to 10.44 eV. One reason for this is that the ion production efficiency is very low near the ionization threshold. Also, hot band effects, ion/molecule reactions, etc. often cause difficulties in the accurate measurement of the AEs for the fragmentations. In the present work, the light source we employed was high-intensity synchrotron radiation, which is especially suitable for the photoionization processes of a molecule. Also, the experiments were carried out under supersonic conditions, thereby overcoming the effects of the aforementioned secondary processes.

In this note, we report the photoionization efficiency (PIE) curves of all ions resulting from the dissociative photoionizations of propylene oxide in the photon energy region of 10−40 eV. From these data, we will attempt to derive the energetics of the dissociations. Combining these results with high-level ab initio calculations, the dissoication channels of propylene oxide can then be established.

Experimental and Computational Methods

The details of the experimental setup[2,8−15] and the computational method employed in this work were described in previous publications.[2,8−11] Hence only a brief account is given below.

Experimental Setup. Synchrotron radiation from the 800 MeV electron storage ring (National Synchrotron Radiation Laboratory, Hefei, Anhui, China) was monochromized by using a 1 m Sega-Namioka monochromator equipped with two gratings (2400 and 1200 lines mm^{-1}) covering the wavelength range from 30 to 300 nm. The gratings were coated with Au and blazed at 60 and 144 nm, respectively. The wavelength resolution was about 0.1 nm with 150 μm entrance and exit slits. The photon flux was monitored by a sodium salicylate coated glass window with a photomultiplier tube behind the

10.1021/jp990635o CCC: $18.00
Published on Web 09/23/1999

ionization chamber. The PIE curves were normalized by the photon flux. In the wavelength region longer than the LiF cutoff wavelength (105 nm), a LiF fitter (thickness 1 mm) was used to eliminate higher order radiation of the dispersed light. The absolute wavelength of the monochromator was calibrated with the known IEs and atomization peaks of the inert gases He, Ne, and Ar.

A homemade TOF mass spectrometer was used for the VUV photoionization and dissociative photoionization studies. The TOF tube was 0.4 m long and its mass resolution was larger than 200. Photoions produced by the VUV light were drawn out of the photoionization region by a transistor-transistor logic (TTL) pulse and detected by a microchannel plate detector. The photoion pulse was used to stop a time-to-amplitude converter (TAC), which was started with the TTL pulse. The output of the TAC was sorted in a multichannel analyzer. A mass spectrum was obtained as the photoion number against the flight time of the ions. The ion signal intensity was controlled so as to avoid the parasitic effect in using the TAC for the TOF measurements. The mass spectral peaks were calibrated with the known m/e ratio of the inert gases Ne and Ar. A specific ion can be selected with the TAC combined with a single-channel analyzer. The PIE curve was obtained as the wavelength was scanned.

Propylene oxide (with 99% purity) was obtained from Shanghai Chemical Reagent Plant (No. 2) and used without further purification. The vapor of propylene oxide was introduced by supersonic expansion through a continuous beam nozzle (70 μm diameter) from the molecule beam chamber into the ionization chamber through a 1.5 mm skimmer. Noble gas He (with 99.999% purity) was used as the carrier gas, and the stagnation pressure was 0.1 MPa. The pressure of the ionization chamber was about 1×10^{-4} Pa when the molecule beam was introduced. No cluster was observed under this condition, so it may be concluded that all fragment ions originated from the dissociative photoionization of propylene oxide.

Computational Method. The Gaussian-2 (G2) theoretical procedure[16] was the high-level ab initio method employed in this work. This method is an approximation for the QCISD(T)/6-311+G(3df,2p) energy. It entails single-point calculations at the MP4/6-311G(d,p), QCISD(T)/6-311G(d,p), MP4/6-311+G(d,p), MP4/6-311G(2df,p), and MP2/6-311+G(3df,2p) levels, all computed with the structures optimized at the MP2(Full)/6-31G(d) level. The HF/6-31G(d) harmonic frequencies, scaled by 0.8929, are used for temperature and zero-point vibrational energy corrections. A small semiempirical correction is also applied to account for the high-level correlation effect. We have applied this method to a variety of chemical systems.[17] The agreement between G2 and experimental results is usually well within $\pm$0.15 eV. All computations involved in this work were carried out on SGI R10000 and DEC 500 au workstations and an SGI Origin 2000 High Performance Server using the Gaussian 94 suite of programs.[18]

In this work, all equilibrium structures and transition structures (TSs) were characterized by the calculations of their vibrational frequencies at both the HF/6-31G(d) and MP2(Full)/6-31G(d) levels. Regarding the TSs, for the simpler cases, the "reactant(s)" and "product(s)" linked by a given TS were confirmed by examining the transition vector of the TS. For the more complicated cases, the "reactant(s)" and "product(s)" were verified by intrinsic reaction coordinate calculations. For those dissociations we claim to involve no TSs, we did attempt to locate the TSs for them and none was found.

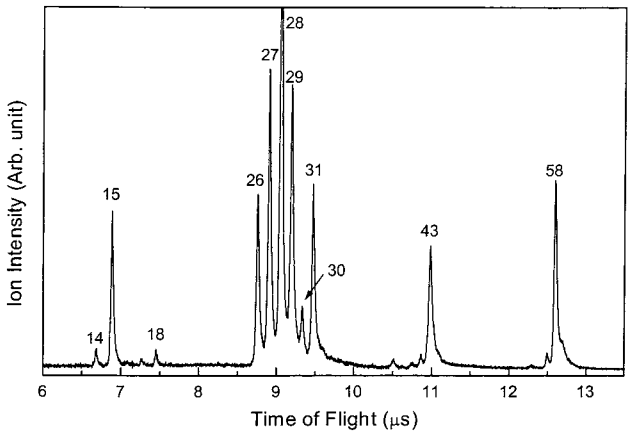

Figure 1. Photoionization time-of-flight mass spectrum of propylene oxide at the wavelength of 30 nm.

TABLE 1: Appearance Energies (eV) and Relative Abundances of the Fragment Ions Measured in the Photodissociation of Propylene Oxide

m/e	ion	relative abundance[a]	this work	EI[b]
58	$C_3H_6O^+$ [c]	36.9	10.21 ± 0.02	9.8
43	$C_2H_3O^+$	24.2	10.79 ± 0.02	10.9
31	CH_3O^+	36.1	13.02 ± 0.03	13.4
30	CH_2O^+	12.5	11.23 ± 0.02	11.6
29	CHO^+	55.3	12.35 ± 0.03	11.8
28	$C_2H_4^+$	100.0	11.23 ± 0.03	11.6
27	$C_2H_3^+$	58.3	13.98 ± 0.03	14.3
26	$C_2H_2^+$	34.1	13.87 ± 0.04	13.9
15	CH_3^+	29.6	13.66 ± 0.03	13.9
14	CH_2^+	4.3	18.13 ± 0.06	18.8

[a] Relative abundances of the fragment ions measured at the wavelength of 30 nm. [b] Data obtained using photoionization techniques, taken from ref 3. [c] Other reported AE values for this ion include 10.1,[5] 10.22,[7] 10.26,[4] and 10.44 eV.[6]

Results and Discussion

Experimental Measurements. We have measured the TOF mass spectra from the photoionization of propylene oxide in the photon energy range from its first ionization potential (~10 eV) to ~40 eV. The typical TOF mass spectrum of propylene oxide at the wavelength 30 nm is shown in Figure 1. In this figure, the mass peak at $m/e = 58$ is the parent ion $C_3H_6O^+$, the other mass peaks at $m/e = 43$, 31, 30, 29, 28, 27, 26, 15, and 14 are the fragment ions listed in Table 1, along with the relative abundances of these ions measured at the wavelength of 30 nm. The mass peak at $m/e = 28$ is the $C_2H_4^+$ ion, which is the highest peak. It shows that the channel of forming the $C_2H_4^+$ ion is the principal dissociative photoionization channel of propylene oxide. Besides, there are some other small mass peaks from propylene oxide. The mass peaks at $m/e = 18$ and 17 were ignored because they arose from the photoionization of the background water molecule in the ionization chamber.

The PIE curves of the parent ion $C_3H_6O^+$, and of the fragment ions $C_2H_3O^+$, CH_3O^+, CH_2O^+, CHO^+, $C_2H_4^+$, $C_2H_3^+$, $C_2H_2^+$, CH_3^+, and CH_2^+ from propylene oxide, were obtained by scanning continuously the wavelength of the grating. Figures 2−5 show, respectively, the PIE spectra of the parent ion $C_3H_6O^+$ and of the other fragment ions. The AE in each PIE curve was determined by the linear extrapolation method.[8,9,19] In arriving at our AE values, we ignored the thermal energy distribution of the parent molecule in our data treatment,[2] considering the present nozzle expansion condition described above.

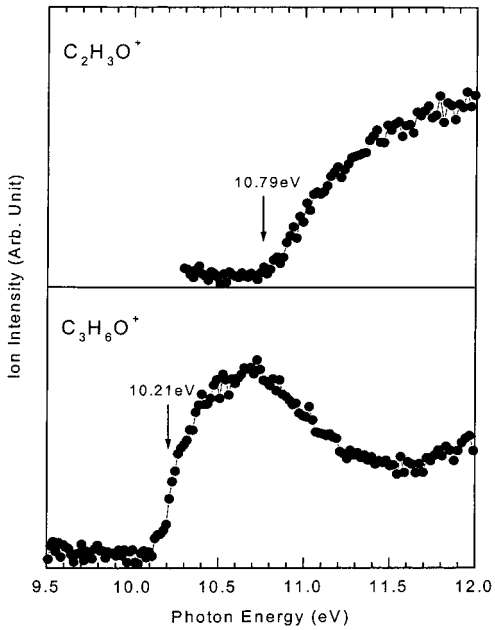

Figure 2. Photoionization yield curve of parent ion $C_3H_6O^+$ and the photoionization efficiency curve of $C_2H_3O^+$ from propylene oxide.

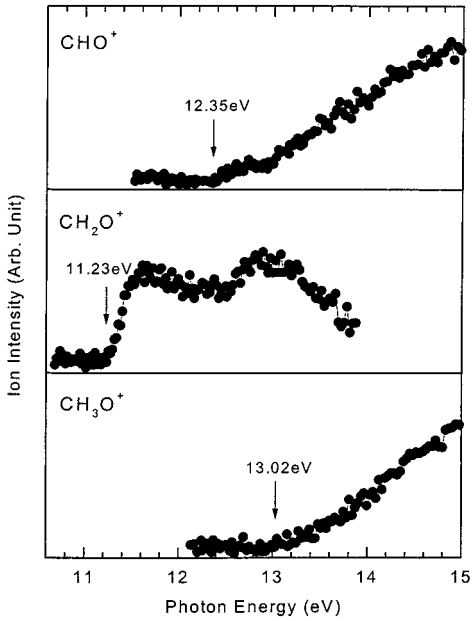

Figure 3. Photoionization efficiency curves of CHO^+, CH_2O^+, and CH_3O^+ from propylene oxide.

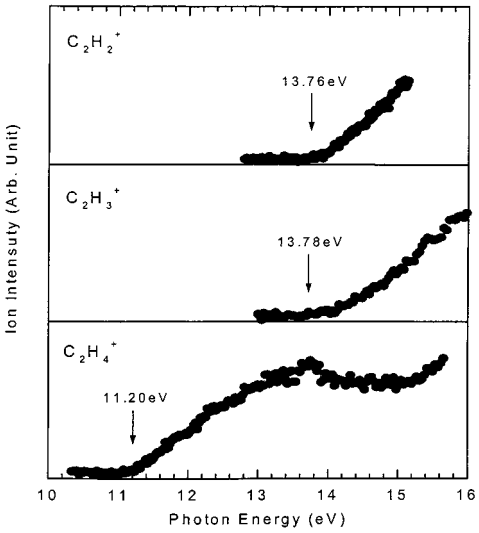

Figure 4. Photoionization efficiency curves of $C_2H_2^+$, $C_2H_3^+$, and $C_2H_4^+$ from propylene oxide.

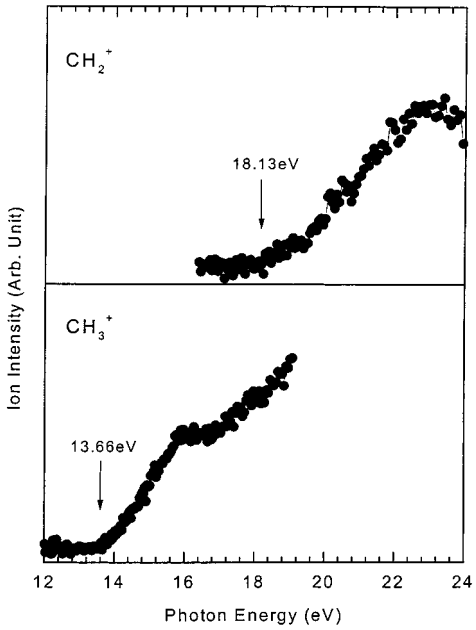

Figure 5. Photoionization efficiency curves of CH_2^+ and CH_3^+ from propylene oxide.

All the AEs for various fragment ions derived from the PIE curves are tabulated in Table 1, along with the error ranges that reflect the bandwidth of our monochromator. Also listed in Table 1 are the AEs obtained using the EI technique.[3] Comparing these two sets of results, it can be seen that the AEs derived from the EI experiments are in general higher than those obtained in this work. It is known that the EI ionization method often overestimates the AEs of both the parent and fragment ions.

The IE of propylene oxide we have measured is a bit lower than most of the reported values in the literature except that of Gallegos and Kiser,[3] as well as that of Aue and Bower.[5] It should be mentioned that in measuring the PIE curves of $C_3H_6O^+$, $C_2H_3O^+$, CH_2O^+, and $C_2H_4^+$, a LiF filter was used to eliminate the effect of higher order radiation from the grating of 1200 lines mm^{-1}. For the AE measurements of CH_3O^+, CHO^+, $C_2H_3^+$, $C_2H_2^+$, CH_3^+, and CH_2^+, the grating of 2400 lines mm^{-1} was used without adding a filter. According to our experience, the effect of the second-order radiation from the grating of 2400 lines mm^{-1} is negligible.[2,8−15] Due to the adoption of the continuously wavelength scanning procedure and the usage of the LiF filter to cut off the higher order radiation, our photoionization onset in the PIE curve of parent ion $C_3H_6O^+$ shown Figure 2 appears quite sharp and clear. In addition, our experiments were carried out under supersonic cooling conditions, thereby overcoming the hot band effect and other adverse influences on the accurate determination of the AEs. We therefore believe that the IE of propylene oxide we have measured is reasonably accurate. The experimental IEs of propylene oxide measured by various groups are 10.1,[5] 10.26,[4] and 10.44 eV,[6] all using photoelectron spectroscopy. There are some differences in the ionization energy values among various groups, although the same experimental method was used. Early

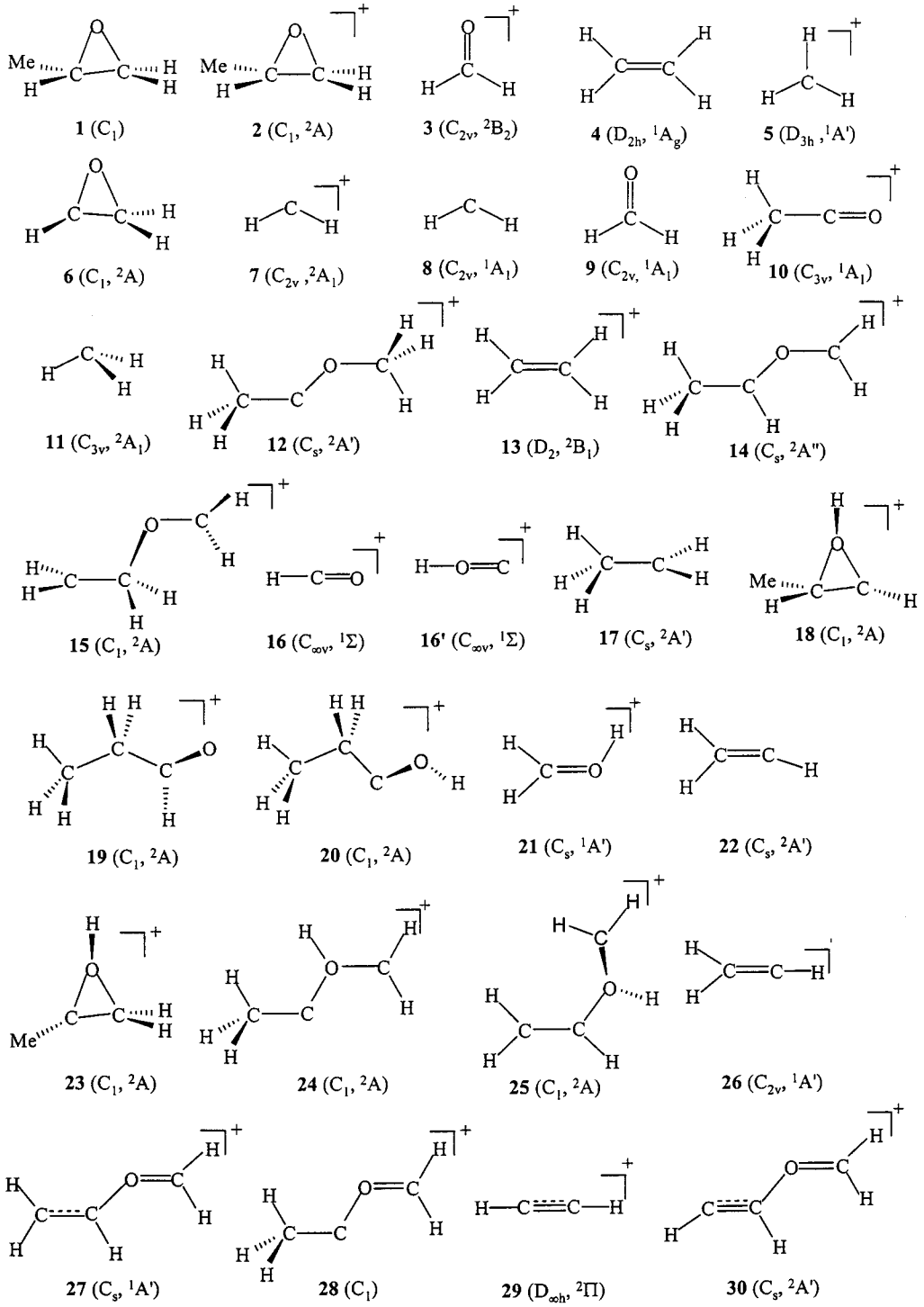

Figure 6. Structural formulas of the various polyatomic species (with three or more atoms) involved in this work, along with their symmetry point groups and electronic states.

IE measurement on propylene oxide by the photoionization method gave a value of 10.22 eV,[7] which is a bit higher than the value measured in this work (10.15 ± 0.02 eV).

In our treatment of the experimental data, we associate the photoionization onset of a fragment ion with the thermochemical origin for that ion. In other words, corrections due to reverse activation barriers and the kinetic shifts have not been made. Since these factors tend to shift the observed onset to higher energies, the photoionization onsets only give upper limits.

We are aware of that in some studies factors such as reverse activation barriers, thermal internal energy, and kinetic shifts have been taken into account. For instance, Smith and Radom[20] have calculated the reverse activation barrier for $CH_3CHO \rightarrow CH_3CO^+ + H + e^-$ to be 14.3 kJ mol^{-1}. Traeger and Kompe[19] have estimated the thermal energy correction for $C_7H_7X + h\nu \rightarrow C_7H_7^+ + X + e^-$ to be 16.9 kJ mol^{-1}. Ruscic and Berkowitz[21] have evaluated the internal energy correction at 0 K for $CH_2S + h\nu \rightarrow CHS^+ + H + e^-$ to be 0.074 eV. Ng and co-workers[22] have calculated the kinetic shift for $CH_3SSCH_3^+ \rightarrow CH_3S_2^+ + CH_3$ to be 0.2 eV. Experimentally, Lifshitz[23] have attempted to overcome kinetic shifts with ion trapping.

On the other hand, in some recent studies, the factors of reverse activation energy and kinetic shifts are ignored. For example, in their photoionization/mass spectroscopic study of

TABLE 2: G2 Energies (E_0), Enthalpies (H_{298}), and Standard Heats of Formation at 298 K ($\Delta H°_{f298}$) of Various Species Involved in the Dissociation of Propylene Oxide and Its Cation

species	E_0(G2) (hartee)	H_{298}(G2) (hartee)	$\Delta H°_{f298}$(G2) (kJ mol^{-1})	$\Delta H°_{f298}$(exp)[b] (kJ mol^{-1})
C_3H_6O (**1**)	−192.76604	−192.76061	−97.6	−94.7 ± 0.6
$C_3H_6O^+$ (**2**)	−192.38700	−192.38112	898.7	891
CH_2O^+ (**3**)	−113.93626	−113.93240	941.1	940.5
C_2H_4 (**4**)	−78.41593	−78.41193	54.2	52.2 ± 1
CH_3^+ (**5**)	−39.38559	−39.38179	1090.0	1093.3 ± 1.7
C_2H_3O (**6**)	−152.86761	−152.86352	165.3	
CH_2^+ (**7**)	−38.69006	−38.68623	1391.6	1386
CH_2 (**8**)	−39.05839	−39.05461	424.5	430.1
CH_2O[a] (**9**)	−114.33892	−114.33510	−116.1	−108.7 ± 0.7
CH_3CO^+ (**10**)	−152.68114	−152.67656	656.1	653
CH_3[a] (**11**)	−39.74509	−39.74084	147.3	145.8
CH_3COCH_3 (**12**)	−192.42476	−192.41780	802.4	
$C_2H_4^+$ (**13**)	−78.02631	−78.02167	1078.8	1066
CH_3CHOCH_2+ (**14**)	−192.42830	−192.42173	792.1	
$CH_2CH_2OCH_2$+ (**15**)	−192.41355	−192.40686	831.1	
HCO^+ (**16**)	−113.40111	−113.39769	820.5	825.6
HOC^+ (**16′**)	−113.34185	−113.33713	979.5	963
C_2H_5 (**17**)	−78.97017	−78.96523	126.0	118
c-$CH(CH_3)OHCH^+$ (**18**)	−192.38597	−192.37995	901.8	
$CH_3CH_2CHO^+$ (**19**)	−192.45348	−192.44721	725.2	*c*
$CH_3CH_2COH^+$ (**20**)	−192.42278	−192.41644	806.0	
CH_2OH^+ (**21**)	−114.60776	−114.60387	702.8	703
C_2H_3 (**22**)	−77.73985	−77.73578	304.8	299 ± 5[d]
c−$C(CH_3)OHCH_2^+$ (**23**)	−192.39068	−192.38476	889.2	
$CH_3COHCH_2^+$ (**24**)	−192.30170	−192.29458	1125.9	
$CH_2CHOHCH_2^+$ (**25**)	−192.38498	−192.37821	906.3	
$C_2H_3^+$ (**26**)	−77.42349	−77.41922	1136.0	*e*
$CH_2CHOCH_2^+$ (**27**)	−191.85591	−191.85020	768.1	
$CH_3COCH_2^+$ (**28**)	−191.75917	−191.75283	1023.7	
$C_2H_2^+$ (**29**)	−76.76599	−76.76229	1336.2	1327.9
$CHCHOCH_2^+$ (**30**)	−191.17020	−191.16444	1044.0	
H[a]	−0.50000			
CO[a]	−113.17749			
H_2[a]	−1.16636			

transition structures[f]	E_0(G2) (hartee)	transition structures[f]	E_0(G2) (hartee)
TSa	−192.35968	TSh	−192.28071
TSb	−192.35999	TSi	−192.28723
TSc	−192.34357	TSj	−192.25026
TSd	−192.33335	TSk	−192.35240
TSe	−192.30351	TSl	−192.25026
TSf	−192.36781	TSm	−191.75751
TSg	−192.34082	TSn	−192.32495

[a] Values taken from ref 16. [b] Unless specified, all experimental ÄH^o_{f298} values are taken from ref 27. [c] There are no experimental data for **19**. On the other hand, the experimental $\Delta H°_{f298}$ for its rotamer with respect to the C−C bond is 772.9 kJ mol^{-1}, which is in good agreement with the G2 result of 785.2 kJ mol^{-1}. [d] Value taken from ref 28. [e] There apparently is no experimental $\Delta H°_{f298}$ for **26**. But for its nonclassical cyclic isomer the experimental $\Delta H°_{f298}$ is 1112 kJ mol^{-1}, which is in good accord with the G2 result of 1117.9 kJ mol^{-1}. [f] The transition structures TSa to TSn are defined in Figures 7−14.

$Si(CH_3)_nH_{4-n}$, Beauchamp et al.[24] used the observed AEs without any correction to derive the dissociation energies $D_0(M^+ - H)$ and $D_0(M^+ - CH_3)$. Also, in the investigation of the photoionization of bromomethanes and iodomethanes, Baer and co-workers[25] derived various heats of formation without regard to possible effects due to kinetic energy release; they pointed out that their results are thus upper limits. Likewise, Lee et al.[26] pointed out that the AE for H^+ of 18.66 eV in the photoionization of C_2H_4 may be regarded as the upper limit of H^+ formation and made no further correction in their determination of C−H bond dissociation energy in C_2H_4. In our previous studies on the photoionization of NH_3,[8] vinyl chloride,[9] carbon tetrachloride,[10] and dichlorodifluoromethane,[11] we also followed this procedure and found the results satisfactory. In the present work, we once again have carried out the same practice, and the various values derived should hence be taken as upper limits. However, as will be seen later, the G2 energies of our proposed dissociation channels are in very good agreement with the experimental measurements. Therefore, the upper limits reported herein should be very close to the actual values.

Computational Results. The structural formulas of the polyatomic species (with three atoms or more) involved in this work, along with their symmetry point groups and electronic states, are shown in Figure 6. The calculated G2 energies, enthalpies, and standard heats of formation at 298 K of all the species involved in the dissociations of propylene oxide (**1**) and its cation (**2**) are listed in Table 2. To gauge the accuracy of the G2 results, we have also tabulated the available experimental heats of formation for easy comparison. On the basis of the E_0(G2) values of **1** and **2** in Table 2, the IE of propylene oxide is calculated to be 10.31 eV. Considering that the error range for G2 results is ±0.15 eV, this calculated value is in fair agreement with the experimental result, 10.15 ± 0.02 eV.

Upon comparing the G2 and experimental heats of formation listed in Table 2, we can see that the agreements are uniformly

TABLE 3: Experimental and Calculated Energies (eV) of the Dissociation of Propylene Oxide Cation

dissociation reaction	ΔE(exp)	ΔE(G2) or reaction barrier
Simple Bond Cleavage Reactions		
(1) $C_3H_6O^+$ (**2**) → CH_2O^+ (**3**) + C_2H_4 (**4**)	1.08 ± 0.02	0.95
(2) $C_3H_6O^+$ (**2**) → CH_3^+ (**5**) + C_2H_3O (**6**)	3.51 ± 0.03	3.64
(3) $C_3H_6O^+$ (**2**) → CH_2^+ (**7**) + CH_2 (**8**) + CO + H_2	7.98 ± 0.06	8.02
or → CH_2^+ (**7**) + CH_2 (**8**) + CH_2O (**9**)		8.15
Reactions Involving Reaction Barriers		
(4) $C_3H_6O^+$ (**2**) → $C_2H_3O^+$ (**10**) + CH_3 (**11**)	0.64 ± 0.02	0.74
(5) $C_3H_6O^+$ (**2**) → $C_2H_4^+$ (**13**) + CH_2O (**9**)	1.08 ± 0.03	1.18
(6) $C_3H_6O^+$ (**2**) → HCO^+ (**16**) + C_2H_5 (**17**)	2.20 ± 0.03	2.27
or → HCO^+ (**16′**) + C_2H_5 (**17**)		
(7) $C_3H_6O^+$ (**2**) → CH_3O^+ (**21**) + C_2H_3 (**22**)	2.87 ± 0.03	2.89
(8) $C_3H_6O^+$ (**2**) → $C_2H_3^+$ (**26**) + CH_2O (**9**) + H	3.83 ± 0.03	3.72
or → $C_2H_3^+$ (**26**) + CO + H_2 + H		
(9) $C_3H_6O^+$ (**2**) → $C_2H_2^+$ (**29**) + CH_2O (**9**) + H_2	3.72 ± 0.04	3.72
or → $C_2H_2^+$ (**29**) + CO + $2H_2$		

good. On the basis of these results, the dissociation channels of **2** can be established with a fair amount of confidence.

Bond Cleavage Reactions. This section summarizes the dissociations of **2,** which entails only bond cleavage(s), i.e., involving no transition states.

$$C_3H_6O^+ (\mathbf{2}) \xrightarrow{\Delta E_1} CH_2O^+ (\mathbf{3}) + C_2H_4 (\mathbf{4}) \qquad (1)$$

$$\Delta E_1 = \mathrm{AE}(CH_2O^+) - \mathrm{IE}(C_3H_6O) = 1.08 \pm 0.02 \text{ eV}$$

$$C_3H_6O^+ (\mathbf{2}) \xrightarrow{\Delta E_2} CH_3^+ (\mathbf{5}) + C_2H_3O (\mathbf{6}) \qquad (2)$$

$$\Delta E_2 = \mathrm{AE}(CH_3^+) - \mathrm{IE}(C_3H_6O) = 3.51 \pm 0.03 \text{ eV}$$

$$C_3H_6O^+ (\mathbf{2}) \xrightarrow{\Delta E_3} CH_2^+ (\mathbf{7}) + CO + H_2 + CH_2 (\mathbf{8}) \qquad (3)$$

$$\Delta E_3 = \mathrm{AE}(CH_2^+) - \mathrm{IE}(C_3H_6O) = 7.98 \pm 0.06 \text{ eV}$$

In the above calculations, the IE of **1** measured in this work is used. The above dissociation energies (ΔE_1 to ΔE_3), along with those calculated by the G2 method (using the data tabulated in Table 2), are given in Table 3 for easy comparison. It is seen that the G2 dissociation energies are in good agreement with the experimental results; i.e., dissociation channels (1)−(3) are supported by high level ab initio results. Still, some uncertainties remain. For instance, the dissociation channel involving CH_2^+ may be

$$C_3H_6O^+ (\mathbf{2}) \xrightarrow{\Delta E_{3'}} CH_2^+ (\mathbf{7}) + CH_2 (\mathbf{8}) + CH_2O (\mathbf{9}) \qquad (3')$$

The G2 dissociation energy for this reaction, $\Delta E_{3'}$, is 8.15 eV. When this value is compared with the experimental result of 7.98 ± 0.06 eV, the agreement is not very good. Nonetheless, reaction 3′ cannot be completely ruled out.

Dissociation Channels Involving Transition Structure(s). In this section, those dissociations involving one or more TSs are discussed.

$$C_3H_6O^+ (\mathbf{2}) \xrightarrow{\Delta E_4} CH_3CO^+ (\mathbf{10}) + CH_3 (\mathbf{11}) \qquad (4)$$

To dissociate into CH_3CO^+ (**10**) and CH_3 (**11**), $C_3H_6O^+$ (**2**) first undergoes hydrogen transfer and ring-opening reaction via TSa to form intermediate cation **12**. Cation **12** then produces **10** and **11** by undergoing a bond cleavage reaction. The schematic energy profile of this process and the structure of TSa are shown in Figure 7. The G2 barrier of this reaction is 0.74 eV, in fair agreement with the experimental dissociation energy, 0.64 ± 0.02 eV.

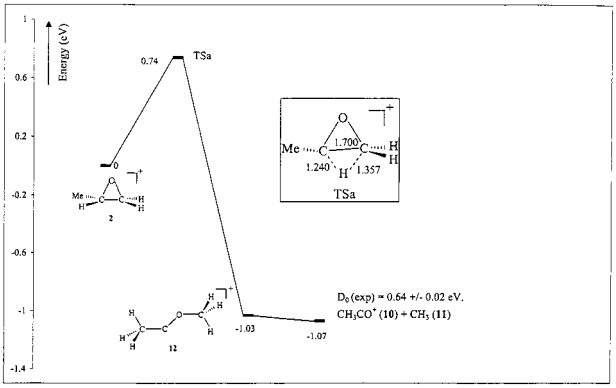

Figure 7. Potential energy surface showing the possible mechanism for dissociation $C_3H_6O^+ \rightarrow C_2H_3O^+ + CH_3$.

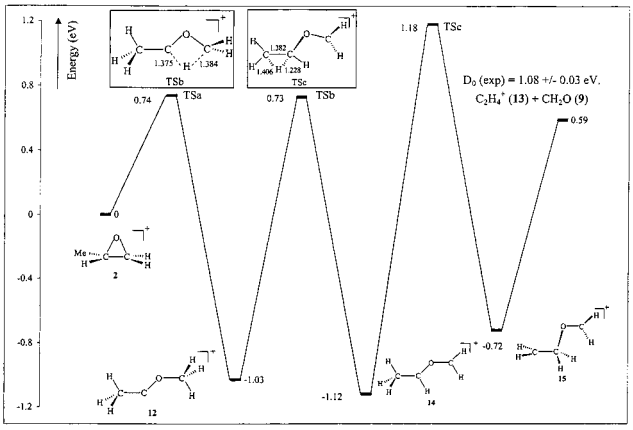

Figure 8. Potential energy surface showing the possible mechanism for dissociation $C_3H_6O^+ \rightarrow C_2H_4^+ + CH_2O$.

$$C_3H_6O^+ (\mathbf{2}) \xrightarrow{\Delta E_5} C_2H_4^+ (\mathbf{13}) + CH_2O (\mathbf{9}) \qquad (5)$$

The energy profile of this reaction is shown in Figure 8. As in reaction 4, cation **12** is first formed via TSa. It then undergoes two successive 1,2-hydrogen transfers via TSb and TSc to form **15**, which produces **13** and **9** by bond cleavage reaction. The

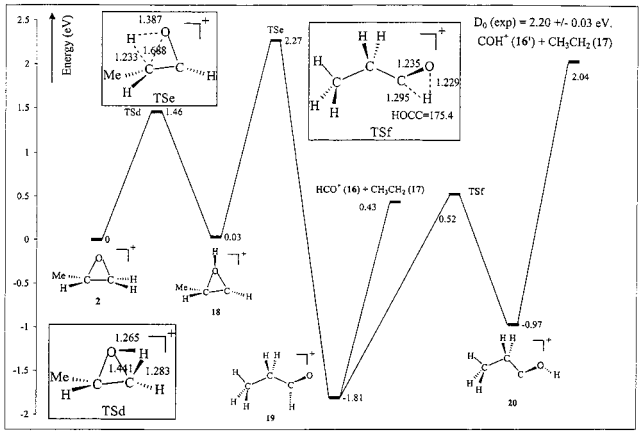

Figure 9. Potential energy surface showing the possible mechanism for dissociation $C_3H_6O^+ \rightarrow HCO^+ + C_2H_5$.

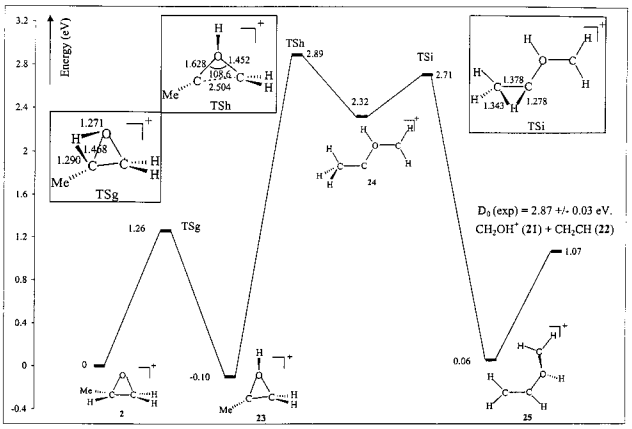

Figure 10. Potential energy surface showing the possible mechanism for dissociation $C_3H_6O^+ \rightarrow CH_3O^+ + C_2H_3$.

G2 barrier of this process is 1.18 eV, again in fair accord with the experimental dissociation energy, 1.08 ± 0.03 eV.

$$C_3H_6O^+ (\mathbf{2}) \xrightarrow{\Delta E_6} HCO^+ (\mathbf{16}) + CH_3CH_2 (\mathbf{17}) \qquad (6)$$

$$C_3H_6O^+ (\mathbf{2}) \xrightarrow{\Delta E_{6'}} COH^+ (\mathbf{16'}) + CH_3CH_2 (\mathbf{17}) \qquad (6')$$

The energy profiles of these two related reactions are shown in Figure 9. The parent cation **2** first undergoes hydrogen transfer via TSd to yield cation **18**; **18** then proceeds to form **19** by another hydrogen transfer and ring opening (via TSe). Simple bond cleavage of **19** forms **16** and **17**. On the other hand **19** can also form **20** by yet another hydrogen transfer; **20** then forms **16′** and **17** by bond cleavage. The overall barrier for these two processes is 2.27 eV, in good agreement with the experimental dissociation energy, 2.20 ± 0.03 eV. Hence, by only the criteria of energy barrier, reactions 6 and 6′ cannot be differentiated. However, as shown by the energy profile in Figure 9, reaction 6 may be favored.

$$C_3H_6O^+ (\mathbf{2}) \xrightarrow{\Delta E_7} CH_2OH^+ (\mathbf{21}) + CH_2CH (\mathbf{22}) \qquad (7)$$

The energy profile of this reaction is shown in Figure 10: **2** undergoes hydrogen transfer to form **23** via TSg; **23** then ring opens to yield **24**; **24** then form **25** by another hydrogen transfer; **25** then cleaves one of its C−O bonds to yield **21** and **22**. Once again, the G2 barrier of this reaction, 2.89 eV, is in very good

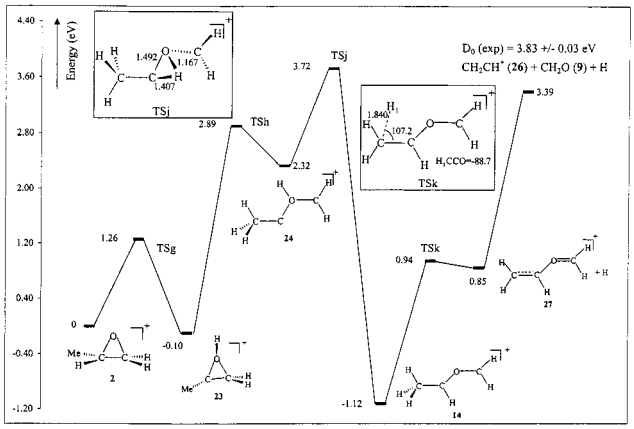

Figure 11. Potential energy surface showing the possible mechanism for dissociation $C_3H_6O^+ \rightarrow C_2H_3^+ + CH_2O + H$.

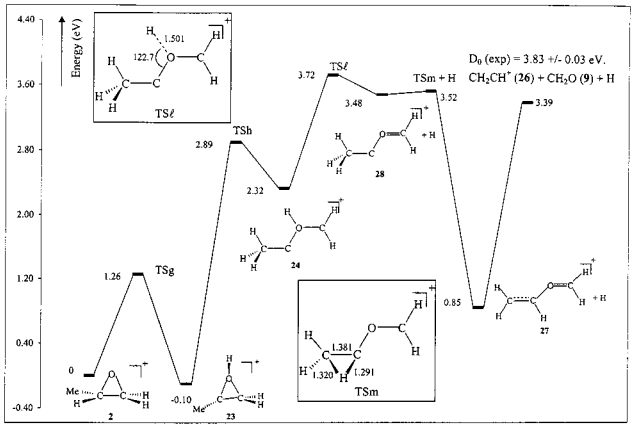

Figure 12. Potential energy surface showing the alternative possible mechanism for dissociation $C_3H_6O^+ \rightarrow C_2H_3^+ + CH_2O + H$.

agreement with the experimental dissociation energy, 2.87 ± 0.03 eV.

$$C_3H_6O^+ (\mathbf{2}) \xrightarrow{\Delta E_8} CH_2CH^+ (\mathbf{26}) + CH_2O (\mathbf{9}) + H \qquad (8)$$

Two pathways are proposed for this reaction; their energy profiles are found in Figures 11 and 12. In both pathways, **2** hydrogen transfers via TSg to form **23**, which then ring opens via TSh to form **24**. As shown in Figure 11, **24** undergoes a 2,3-hydrogen transfer (via TSj) to yield **14**, an intermediate we first encountered in reaction 5 (Figure 12). Cation **14** can form **27** and H by bond cleavage; then **27** further dissociates to yield **26** and **9**. The G2 barrier of this reaction is 3.72 eV, in fair agreement with the experimental dissociation energy, 3.83 ± 0.03 eV.

In the alternative pathway schematically shown in Figure 12, upon its formation, intermediate **24** dissociates into **28** and H via TS*l*. Cation **28** then hydrogen transfers to form **27**, which then yields **26** and **9** by bond cleavage. The overall barrier of this pathway is the same as that for the pathway shown in Figure 11. Hence, it is not obvious which pathway is favored.

$$C_3H_6O^+ (\mathbf{2}) \xrightarrow{\Delta E_9} CHCH^+ (\mathbf{29}) + CH_2O (\mathbf{9}) \qquad (9)$$

Once again, there are two proposed pathways for this reaction and these pathways are schematically shown in Figures 13 and 14. The first portion of Figure 13 is the same as that of Figure 11. Upon forming intermediate **27** plus H, a hydrogen extraction

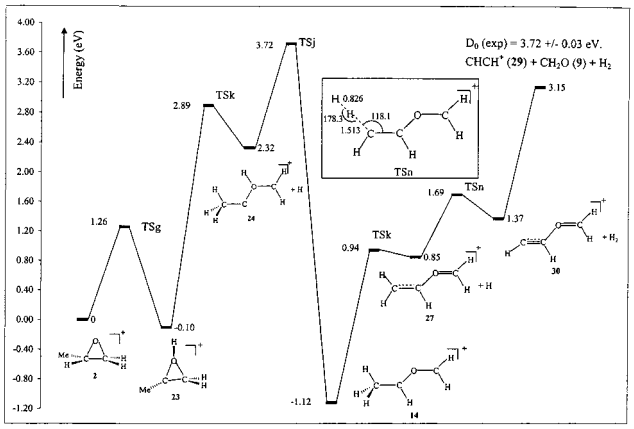

Figure 13. Potential energy surface showing the possible mechanism for dissociation $C_3H_6O^+ \rightarrow C_2H_2^+ + CH_2O + H_2$.

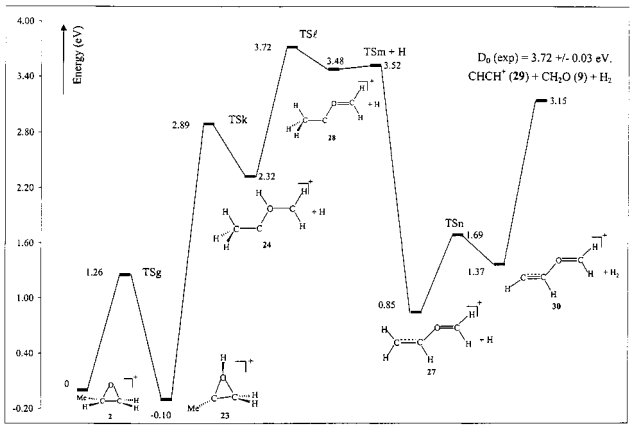

Figure 14. Potential energy surface showing the alternative possible mechanism for dissociation $C_3H_6O^+ \rightarrow C_2H_2^+ + CH_2O + H_2$.

reaction between **27** and H via TSn produces H_2 and **30**. Cation **30** then forms $CHCH^+$ (**29**) and CH_2O (**9**) by bond cleavage. The G2 barrier for this reaction is 3.72 eV, in excellent agreement with the experimental dissociation energy, 3.72 ± 0.04 eV.

In the alternative pathway, shown schematically in Figure 14, **27** plus H is produced in the manner depicted in Figure 12. Once these fragments are formed, they undergo the same hydrogen extraction via TSn to form **30** plus H_2. Cation **30** then produces **29** and **9** by bond cleavage. It is not clear which of these two pathways is favored.

The dissociation energies and the G2 barriers for reactions 4−9 are included in Table 3 for ready comparison. As can be seen from these results, the agreements between theory and experiment are uniformly good.

Conclusions

By combining the techniques of synchrotron radiation and molecular beam and mass spectrometry, we have measured the AEs of $C_3H_6O^+$, $C_2H_3O^+$, CH_3O^+, CH_2O^+, CHO^+, $C_2H_4^+$, $C_2H_3^+$, $C_2H_2^+$, CH_3^+, and CH_2^+ in the dissociation of propylene oxide. With the aid of ab initio Gaussian-2 results, we have attempted to establish the dissociation channels for the formation of these fragments. The dissociation channels we have proposed include simple bond cleavage reactions and processes involving reaction intermediates and transition structures. The agreements between experimental and computational dissociation energies or barriers are well within ±0.15 eV.

Acknowledgment. W.K.L. and K.C.L. are grateful to the Computer Services Center at the Chinese University of Hong Kong for generous allocation of computation time on the SGI Origin 2000 High Performance Server. This project (No. 29673037) is partially supported by the National Natural Science Foundation of China.

References and Notes

(1) Hua, W. *Heterocyclic Chemistry*; Peking University Press: Beijing, 1991 (in Chinese).

(2) Liu, F.; Qi, F.; Gao, H.; Sheng, L.; Zhang, Y.; Yu, S.; Lau, K.-C.; Li, W.-K. *J. Phys. Chem. A* **1999**, *103*, 4155.

(3) Gallegos, E. J.; Kiser, R. W. *J. Am. Chem. Soc.* **1961**, *83*, 773.

(4) McAlduff, E. J.; Kiser, R. W. *Can. J. Chem.* 1**997**, *55*, 318.

(5) Aue, D. H.; Bowers, M. T. In *Gas-Phase Ion Chemistry*; Bowers, M. T., Ed.; Academic Press: New York, 1979; Chapter 9.

(6) Kimura, K.; Katsumata, S.; Achiba, Y.; Yamazaki, T.; Iwata, S. *Handbook of HeI Photoelectron Spectra of Fundamental Organic Compounds*; Japan Scientific Society Press: Tokyo, 1981.

(7) Watanabe, K.; Nakayama, T.; Mottle, J. *J. Quantum Spectrrosc. Radiative Transfer* **1962**, *2*, 369.

(8) Qi, F.; Sheng, L.; Zhang, Y.; Yu, S.; Li, W.-K. *Chem. Phys. Lett.* **1995**, *234*, 450.

(9) Sheng, L.; Qi, F.; Tao, L.; Zhang, Y.; Yu, S.; Wong, C.-K.; Li. W.-K. *Int. J. Mass. Spectrom. Ion Processes* **1995**, *148*, 179.

(10) Li, Q.; Ran, Q.; Chen, C.; Yu, S.; Ma, X.; Sheng, L.; Zhang, Y.; Li, W.-K. *Int. J. Mass Spectrom. Ion Processes* **1996**, *153*, 29.

(11) Sheng, L.; Qi, F.; Gao, H.; Zhang, Y.; Yu, S.; Li, W.-K. *Int. J. Mass Spectrom. Ion Processes* **1997**, *161*, 151.

(12) Zhang, Y.; Sheng, L.; Gao, H.; Qi, F. In *Atomic and Molecular Photoionization*; Yagishita, Y., Sasaki, T., Eds.; Universal Academy: New York, 1996; pp 197−204.

(13) Qi, F.; Yang, S.; Sheng, L.; Ye, W.; Gao, H.; Zhang, Y.; Yu, S. *J. Phys. Chem. A* **1997**, *101*, 7194.

(14) Qi, F.; Yang, X.; Yang, S.; Gao, H.; Sheng, L.; Zhang, Y.; Yu, S. *J. Chem. Phys.* **1997**, *107*, 4911.

(15) Qi, F.; Yang, S.; Sheng, L.; Gao, H.; Zhang, Y.; Yu, S. *J. Chem. Phys.* **1997**, *107*, 10391.

(16) Curtiss, L. A.; Raghavachari, K.; Trucks, G. W.; Pople, J. A. *J. Chem. Phys.* **1991**, *94*, 7221.

(17) Lau, K.-C.; Li, W.-K.; Ng, C. Y.; Chiu, S.-W. *J. Phys. Chem. A* **1999**, *103*, 3330 and references cited therein.

(18) Frisch, M. J.; Trucks, G. W.; Schlegel, H. B.; Gill, P. M. W.; Johnson, B. J.; Robb, M. A.; Cheeseman, J. R.; Keith, T. A.; Petersson, G. A.; Montgomery, J. A.; Raghavachari, K.; Al-Laham, M. A.; Zarkrewski, V. G.; Ortiz, J. V.; Foresman, J. B.; Cioslowski, J.; Stefanov, B. B.; Nanayakkara, A.; Challacombe, M.; Peng, C. Y.; Ayala, P. Y.; Chen, W.; Wong, M. W.; Andres, J. L.; Replogle, E. S.; Gomperts, R.; Martin, R. L.; Fox, D. J.; Binkley, J. S.; Defrees, D. J.; Baker, J.; Stewart, J. J. P.; Head-Gordon, M.; Gonzalez, C.; Pople, J. A. *GAUSSIAN* 94, Revision D4; Gaussian, Inc.: Pittsburgh, PA, 1995.

(19) Traeger, J. C.; Kompe, B. W. *Int. J. Mass Spectrom. Ion Processes* **1990**, *101*, 111.

(20) Smith, B. J.; Radom, L. *Int. J. Mass Spectrom. Ion Processes* **1990**, *101*, 209.

(21) Ruscic, B.; Berkowitz, J. *J. Chem. Phys.*. **1993**, *98*, 2568.

(22) Ma, Z.-X.; Liao, C.-L.; Ng, C. Y.; Cheung, Y.-S.; Li, W.-K.; Baer, T. *J. Chem. Phys.* **1994**, *100*, 4870.

(23) Lifshitz, C. *Int. J. Mass Spectrom. Ion Processes* **1991**, *106*, 159.

(24) Shin, S. K.; Corderman, R. R.; Beauchamp, J. L. *Int. J. Mass Spectrom. Ion Processes* **1990**, *101*, 257.

(25) Tsai, B. P.; Baer, T.; Werner, A. S.; Lin, S. F. *J. Chem. Phys.* **1975**, *79*, 570.

(26) Shiromaru, H.; Achiba, Y.; Kimura, K.; Lee, Y. T. *J. Phys. Chem.* **1987**, *91*, 17.

(27) Lias, S. G.; Bartmess, J. E.; Liebman, J. F.; Holmes, J. L.; Levin, R. D.; Mallard, W. G. *J. Phys. Chem. Ref. Data* **1988**, *17*, Suppl. 1.

(28) Tsang, W. In *Energetics of Organic Free Radicals*; Martinho Simoes, J. A., Greenberg, A., Liebman, J. F., Eds.; Blackie Academic and Professional: London, 1996; pp 22−58.